Antiferromagnetic resonance in Rb_2MnCl_4

1994 J. Phys.: Condens. Matter 6 545

(http://iopscience.iop.org/0953-8984/6/2/024)

J. Phys.: Condens. Matter 6 (1994) 545–550. Printed in the UK

Antiferromagnetic resonance in Rb_2MnCl_4

M Hagiwara†, K Katsumata† and J Tuchendler‡

† The Institute of Physical and Chemical Research (RIKEN), Wako, Saitama 351-01, Japan
‡ Laboratoire de Dispositifs Infra-rouge, Université Paris VI, 4 Place Jussieu, 75252 Paris Cédex 05, France

Received 27 August 1993, in final form 5 October 1993

Abstract. Antiferromagnetic resonance (AFMR) experiments on a single-crystal sample of Rb_2MnCl_4 have been performed using a spectrometer with wide frequency and magnetic field ranges. All the AFMR modes predicted for a uniaxial antiferromagnet have been observed. We find a significant contribution of the non-linear term in the expression of the AFMR frequency to the temperature dependence of the resonance point in the high-field low-frequency region.

1. Introduction

Antiferromagnetic resonance (AFMR) has been widely used to study the magnetic properties of antiferromagnets at a microscopic level. From AFMR measurements, one can obtain information about the exchange and anisotropy energies of the materials studied (Nagamiya *et al* 1955, Foner 1963). Originally, in the 1950s the frequency of the apparatus was limited to about 10 GHz and the magnetic field to about 1 T. Therefore, the materials studied were limited to those with a weak exchange interaction, i.e. with a low Néel temperature T_N. It is now possible to have centimetre, millimetre and submillimetre waves ranging from about 1 to about 600 GHz using, for example, klystrons and Carcinotrons (trade name for backward-wave oscillators of Thomson Co.) and up to about 7 THz using a far-infrared laser. Stable high magnetic fields up to 20 T are now available with a superconducting magnet.

In the Institute of Physical and Chemical Research (RIKEN) we are building an electron spin resonance (ESR) spectrometer with wide frequency and field ranges. To test our apparatus, we have tried an AFMR measurement on Rb_2MnCl_4, an antiferromagnet with a relatively strong exchange interaction. Although studied earlier in limited ranges of frequencies and fields (Katsumata *et al* 1984, Katsumata and Tuchendler 1987), AFMR experiments in wider frequency and field ranges could enable us to observe all the AFMR modes expected from the theory (Nagamiya *et al* 1955, Foner 1963). In fact, in the present study we have been able to observe all the AFMR modes in Rb_2MnCl_4. Moreover, we have found a significant contribution of the non-linear term in the expression for the AFMR frequency to the temperature dependence of the resonance point in the high-field low-frequency region.

The format of this paper is as follows. In section 2 we describe the crystal and magnetic structures of Rb_2MnCl_4. Experimental details are given in section 3. In section 4 we present the results of the AFMR experiments and their analysis.

0953-8984/94/020545+06$07.50

2. Crystal and magnetic structures of Rb_2MnCl_4

The crystal structure of Rb_2MnCl_4 belongs to the tetragonal space group D_{4h}^{17} ($I4/mmm$) with two molecules per unit cell. The lattice constants at room temperature are $a = 5.05$ Å and $c = 16.18$ Å (Epstein *et al* 1970). From the neutron scattering study of Epstein *et al* (1970), a ridge characteristic of a two-dimensional antiferromagnet was observed below about 180 K. The compound orders antiferromagnetically below T_N ($\simeq$ 55 K) in a magnetic cell with four molecules per unit. In the ordered phase, the spins in a c plane point antiparallel to their neighbouring spins and the spin structure in the adjacent layer is obtained with the translation $(\frac{1}{2}, \frac{1}{2}, \frac{1}{2})$. The easy axis of the spin of this crystal is determined to be along the c axis. The main origin of the magnetic anisotropy comes from the dipole–dipole interaction (Epstein *et al* 1970).

3. Experimental details

3.1. Sample preparation and characterization

The single crystal of Rb_2MnCl_4 used in the present experiment was grown by the same method described earlier (Katsumata and Tuchendler 1987).

We have measured the temperature dependence of the magnetization M in a single-crystal sample of Rb_2MnCl_4 under an external magnetic field H using a Quantum Design MPMS2 SQUID magnetometer. The result is shown in figure 1. Here, the susceptibility is given by M/H. There is no anisotropy in the susceptibility along the c axis ($\chi_\parallel$) and c plane ($\chi_\perp$) above about 60 K. On the other hand, $\chi_\parallel$ and $\chi_\perp$ behave quite differently below about 60 K. From this measurement we determined the value of T_N to be approximately 60 K, which is consistent with the result of the neutron scattering study (Epstein *et al* 1970).

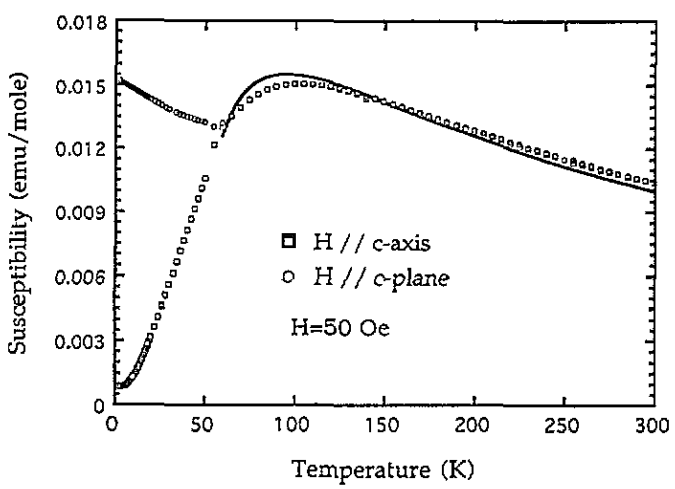

Figure 1. Temperature dependence of the molar magnetic susceptibilities parallel and perpendicular to the c axis of Rb_2MnCl_4 *measured at 50 Oe:* ——, *theoretical curve discussed in the text.*

We have analysed the susceptibility above T_N using the theory developed by Katsumata (1977). Since Mn^{2+} has a spin quantum number $S = \frac{5}{2}$, we may approximate the spin operator as a classical vector. In this case, the susceptibility χ of a square-lattice magnet with nearest-neighbour interaction only is expressed as

$$\chi = [N^2 g^2 \mu_B^2 S(S+1)/k_B T][a_0(T) + a_1(T)\kappa + a_2(T)\kappa^2 + a_3(T)\kappa^3 + \ldots] \qquad (1)$$

where N^2 is the number of Mn^{2+} ions in the sample, g is the g-value of Mn^{2+} spin, μ_B is the Bohr magneton, k_B is Boltzmann's constant and T is the temperature. The coefficients of equation (1) are given by

$$a_0(T) \equiv (1+u)/3(1-u) \qquad a_1(T) \equiv 2(1+u)^2/9(1-u)^2$$

$$a_2(T) \equiv 2(1+u)^3/27(1-u)^3 + \{4u(1+u+u^2)/[27(1+u)^2(1-u)^2]\} \times [(1+u-2u^2)/(1-u) + 2v(1+u+u^2)/(1-uv)]$$

$$\begin{aligned} a_3(T) \equiv \tfrac{1}{6}[[&-184u^6 - 400u^5 - 8u^4 + 448u^3 + 520u^2 + 176u + 8]/[135(1+u)^2(1-u)^4] \\ &+ [192u^7v^4 - 144u^7v^2 + 768u^6v^4 - 128u^6v^3 - 720u^6v^2 + 128u^6v \\ &+ 1296u^5v^4 - 800u^5v^3 - 1248u^5v^2 + 704u^5v + 1296u^4v^4 - 1280u^4v^3 \\ &- 1248u^4v^2 + 1184u^4v + 768u^3v^4 - 1408u^3v^3 - 720u^3v^2 + 1312u^3v \\ &+ 192u^2v^4 - 832u^2v^3 - 144u^2v^2 + 736u^2v - 256uv^3 + 48uv^2 + 256uv \\ &+ 48v^2]/[135(1+u)^2(1-u)^3(1-v^2)(1-uv)^2]] \end{aligned}$$

where $u \equiv \coth\kappa - 1/\kappa$, $v \equiv 1 - 3u/\kappa$, $\kappa \equiv 2JS(S+1)/k_BT$ and J is the exchange constant. To compare the theory with the experiment, we use the value $J/k_B = -5.61$ K which was determined from the neutron scattering study (Schröder *et al* 1980) and $g = 2.00$ which was obtained from the ESR measurement (Katsumata *et al* 1984). As is seen from figure 1, the agreement between theory and experiment is satisfactory without any adjustable parameter.

3.2. *ESR measurements*

The ESR spectrometer consists of two main parts (a magnet and a microwave source) and measuring instruments. The microwaves are generated from three klystrons at the frequencies 20 GHz, 50 GHz and 90 GHz, respectively, and two Carcinotrons operating at the frequencies 200 GHz and 300 GHz, respectively. The magnetic field is produced by a superconducting magnet from Oxford Instruments. The magnetic field can be swept up to 14 T at 4.2 K and up to 16 T at 2.2 K. A Dewar (variable-temperature insert) is used to change the temperature of the sample space from 1.6 to 300 K. The experimental set-up at the high frequencies above 90 GHz is essentially the same as that reported previously (Tuchendler *et al* 1979). At lower frequencies, a conventional cryostat with a resonant cavity is used. The temperature of the sample is measured with a calibrated carbon glass thermometer placed close to it. The ESR measurement is fully automated by the use of a Hewlett–Packard 9000-360CH computer.

4. Experimental results and analysis

We show in figure 2 typical examples of the ESR signal for a Rb_2MnCl_4 single crystal obtained at different frequencies and temperatures when the external magnetic field is applied along the c axis.

Figure 3 summarizes all the AFMR data obtained at low temperatures in the frequency ν versus magnetic field H plane. It is immediately clear that Rb_2MnCl_4 shows the expected AFMR modes typical of a uniaxial antiferromagnet.

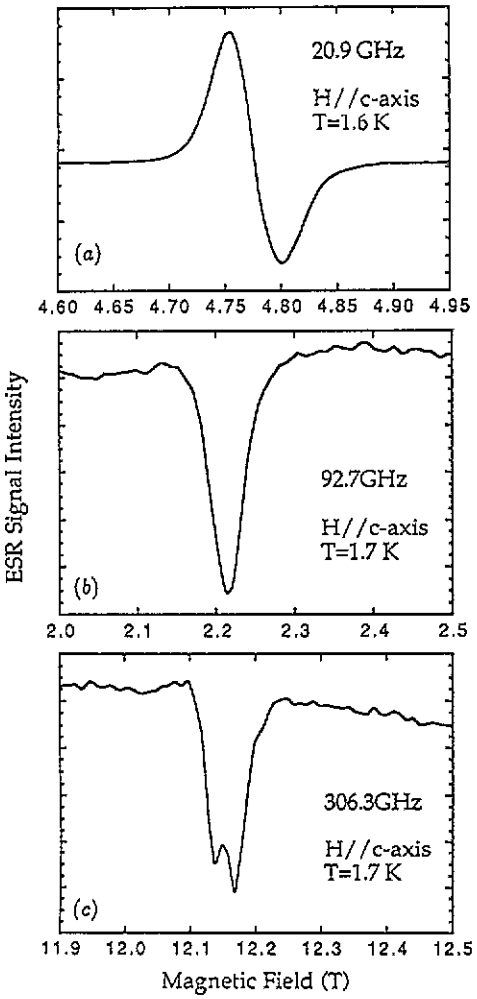

Figure 2. Typical examples of the ESR signal obtained at (*a*) 20.9 GHz, (*b*) 92.7 GHz and (*c*) 306.3 GHz when the external magnetic field is applied to the *c* axis. In the case of 20.9 GHz the derivative of the signal with respect to magnetic field is shown, while the others show the direct absorption curve.

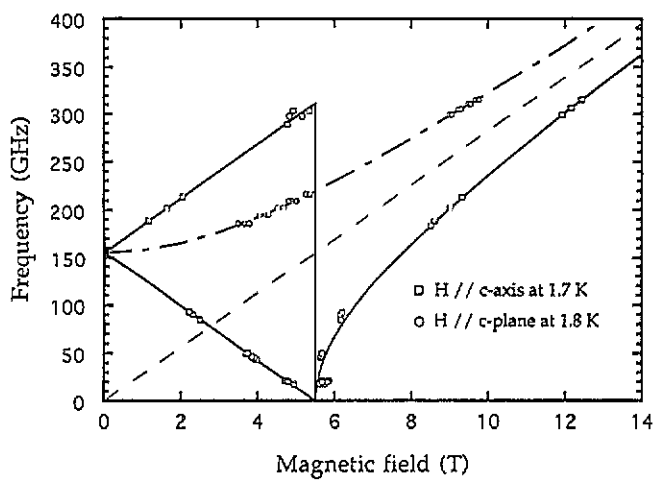

Figure 3. Frequency versus external magnetic field relations of the AFMR signals in Rb_2MnCl_4: ——, — · —, theoretical data discussed in the text.

We have measured the temperature dependence of the resonance field in one of the AFMR modes at fixed frequencies, as shown in figure 4. The behaviour at 90.5 GHz is conventional in which the resonance field decreases with increasing temperature. The behaviour observed at 51.3 GHz is almost the same as that at 90.5 GHz. These observations are consistent with the results reported by Strobel and Geick (1981). On the contrary, the resonance field at 20.3 GHz increases with increasing temperature up to about 25 K and begins to decrease as the temperature increases further.

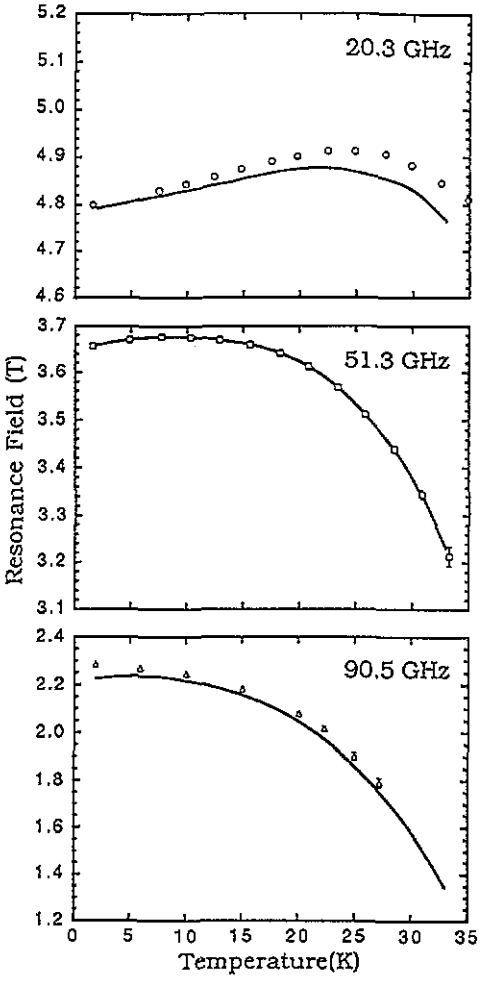

Figure 4. Temperature dependence of the AFMR position at the fixed frequencies: ——, theoretical curves discussed in the text.

In the following, we analyse the experimental results shown in figures 3 and 4. If the exchange field H_E is much larger than the anisotropy field H_A, the AFMR frequencies of a uniaxial antiferromagnet are given by the following equations (Nagamiya *et al* 1955, Foner 1963) (in Rb_2MnCl_4, $H_E \simeq 10^2$ T and $H_A \simeq 0.1$ T so that $H_E \gg H_A$ (Katsumata and Tuchendler 1987)):

$$h\nu/g\mu_B = \sqrt{2K_u/\chi_\perp + (\chi_\parallel H/2\chi_\perp)^2} \pm H(1 - \chi_\parallel/2\chi_\perp) \qquad (\boldsymbol{H} \| c,\ H < H_{SF}) \tag{2}$$

$$h\nu/g\mu_B = \sqrt{H^2 - 2K_u/\chi_\perp} \qquad (\boldsymbol{H} \| c,\ H > H_{SF}) \tag{3}$$

$$h\nu/g\mu_B = \sqrt{H^2 + 2K_u/\chi_\perp} \qquad (H \perp c) \tag{4}$$

where h is Planck's constant, K_u the anisotropy constant and H_{SF} the critical field for spin flop. At low temperatures ($T \ll T_N$), $\chi_\parallel$ is much smaller than $\chi_\perp$, so that equation (2) becomes

$$h\nu/g\mu_B = \sqrt{2K_u/\chi_\perp} \pm H. \tag{5}$$

The two full straight lines below 5.5 T in figure 3 represent equation (5), the full curve above 5.5 T equation (3) and the chain curve equation (4) with $\sqrt{2K_u/\chi_\perp} = 5.51$ T. This value of the zero-field-gap frequency is the same as that reported before (Katsumata *et al* 1984). We see in figure 3 good agreement between theory and experiment. In the present experiment we are able to observe all the AFMR modes predicted by the theory.

Next, we analyse the temperature dependence of the resonance field (figure 4). The frequency versus field relation of the AFMR mode relevant to the data in figure 4 is given by equation (2) with the minus sign. In this equation, K_u, $\chi_\parallel$ and $\chi_\perp$ depend on temperature. We use for the temperature dependence of the ratio $\chi_\parallel/\chi_\perp$ the experimental value deduced from figure 1. We have only one adjustable parameter, $K_u/\chi_\perp$. We obtain the temperature dependence of $K_u/\chi_\perp$ by fitting equation (2) with the data obtained at 51.3 GHz. We can then compare the theory with the experiments performed at 20.3 and 90.5 GHz without any adjustable parameter. In the case of 90.5 GHz the agreement is satisfactory. Although at 20.3 GHz the agreement between the theory and the experiment is not as good as that at 90.5 GHz, the theory reproduces the broad peak at around 25 K. This broad peak in the temperature dependence of the resonance field comes from the combined effect of the two terms $2K_u/\chi_\perp$ and $(\chi_\parallel H/2\chi_\perp)^2$ in equation (2). At higher frequencies the resonance field is lower in this AFMR mode, so that the first term dominates. At lower frequencies the resonance field is higher and the latter term becomes important.

In conclusion, the present experiment performed at high fields demonstrates clearly the effect of the non-linear term on the temperature dependence of the AFMR position, whereas little had been reported so far about the effect of the non-linear term.

Acknowledgments

This work was partially supported by a Grant-in-Aid for Scientific Research from the Japanese Ministry of Education, Science and Culture and by a Grant from the Yazaki Memorial Foundation for Science and Technology.

References

Epstein A, Gurewitz E, Makovsky J and Shaked H 1970 *Phys. Rev.* B **2** 3703–6
Foner S 1963 *Magnetism* vol 1, ed G T Rado and H Suhl (New York: Academic) pp 383–447
Katsumata K 1977 *Solid State Commun.* **23** 481–5
Katsumata K and Tuchendler J 1987 *J. Phys. C: Solid State Phys.* **20** 4873–9
Katsumata K, Tuchendler J and Tanimoto M 1984 *Solid State Commun.* **50** 193–6
Nagamiya T, Yosida K and Kubo R 1955 *Adv. Phys.* **4** 1–112
Schröder B, Wagner V, Lehner N, Kesharwani K M and Geick R 1980 *Phys. Status Solidi* b **97** 501–11
Strobel K and Geick R 1981 *Physica* B **108** 951–2
Tuchendler J, Magarino J and Renard J P 1979 *Phys. Rev.* B **20** 2637–42